

Curvature Estimation in Oriented Patterns Using Curvilinear Models Applied to Gradient Vector Fields

Joost van de Weijer, Lucas J. van Vliet,
Piet W. Verbeek, and
Michael van Ginkel, *Member, IEEE*

Abstract—Curved oriented patterns are dominated by high frequencies and exhibit zero gradients on ridges and valleys. Existing curvature estimators fail here. The characterization of curved oriented patterns based on translation invariance lacks an estimation of local curvature and yields a biased curvature-dependent confidence measure. Using parameterized curvilinear models we measure the amount of local gradient energy along the model gradient as a function of model curvature. Minimizing the residual energy yields a closed-form solution for the local curvature estimate and the corresponding confidence measure. We show that simple curvilinear models are applicable in the analysis of a wide variety of curved oriented patterns.

Index Terms—Oriented patterns, anisotropy, curvature, confidence measures, curvilinear models, gradient vector fields.

1 INTRODUCTION

RELIABLE estimation of local features in digitized images is of great importance for many image processing tasks (segmentation, analysis, and classification). Depending on the class of images under investigation, knowledge of different features is desired. One such class of images is defined by Kass and Witkin [1] as oriented patterns: patterns that exhibit a dominant local orientation. Examples are seismic, acoustic, wood grain, interference patterns, and fingerprint images. Important features for these images are estimates of local anisotropy, orientation, curvature, and scale.

The structure tensor yields a robust estimator for local orientation [1], [2], [3], [4] based on a local gradient vector field. This estimator locally models the images as translation invariant strokes. In addition to orientation estimation, this method also yields an anisotropy measure indicating the resemblance of the local area to a translation invariant model. This measure can also be interpreted as a confidence measure of the estimated orientation. Both a lack of smoothness (e.g., caused by noise) and deviations from the translation invariant model (e.g., curved oriented patterns) are responsible for a decrease of this confidence measure. To distinguish between the two possible causes, we proposed a parabolic transformation which optimizes the translation invariance after transformation [5]. This method yields a curvature estimate for curved oriented patterns as a by-product. A shortcoming of this method is that the proposed transformation is

not orthonormal and, therefore, it lacks conservation of gradient energy. This does not allow direct comparison of the confidence values of different transformations. In this paper, we propose a method to investigate the resemblance of a local pattern of 2D oriented pattern to a certain model function (e.g., circular, parabolic). The model is represented by a parameterized transformation function of the isophotes. The method assures the conservation of gradient energy, allowing us to compare confidence measures of different transformations and, especially, of a parameterized transformation for different parameter values. As in [5], solving the parameter for best confidence yields a closed-form estimate of the additional free parameter, e.g., local curvature. We propose two curvilinear models, a parabolic and a circular model, for the characterization of curved oriented patterns. When the resemblance between a model and a local image is high, the corresponding model parameters, orientation, and curvature yield a reliable description of the local image. The method yields features with a corresponding confidence value. All these estimates are local and can be represented as feature maps.

Estimation of the curvature in oriented patterns is not trivial. Worring and Smeulders [6] presented an extensive comparison between curvature estimators applied to segmented data for which the position and ordering of points along the contour have to be known. For noisy oriented patterns, segmentation fails, making these methods useless. The isophote (tangential) curvature (the second derivative along the isophote divided by the gradient magnitude) and the normal curvature [17] are segmentation-free [7], [8], [17], but also fail on these images. There are three reasons for this [5]: 1) The gradient is zero on ridges and in valleys. 2) Increasing the regularization scale of directional derivatives suppresses the oriented pattern and reduces the signal-to-noise ratio. 3) Opposite sides of a ridge (or valley) yield curvatures of opposite sign which cancel out after averaging. The only two methods which do yield a curvature estimate for oriented patterns are either very computationally demanding [9] or are not accompanied by a confidence measure, which makes them hard to rely on [10].

The proposed method resembles a method for the detection of complex symmetries as presented by Bigün et al. [11], [12], [13]. They characterize symmetries by (coordinate) transformation functions which transform symmetric patterns into translation invariant patterns. The success of such a transformation is determined by the confidence measure of the structure tensor applied to the transformed image. A high confidence value is an indicator for the presence of the corresponding symmetry. Bigün et al. method is an extension of the generalized Hough transform. Detection of a symmetry pattern involves accumulation of evidence by voting. Bigün's symmetry detector requires two orthonormal transformation functions. It measures the resemblance of the local differential field to two perpendicular differential fields (indicating the symmetry), whereas our method looks at the resemblance of the local differential field to only one differential field (representing the shape of the isophotes). This difference allows us to estimate model parameters by optimizing the resemblance between the actual differential field and a model differential field in a closed-form solution, i.e., omitting a time, consuming voting scheme. This is not possible with the symmetry method since neither one of the two differential fields is preferred.

- J. van de Weijer is with the ISIS group of the Faculty of Science, University of Amsterdam, Kruislaan 403, 1098 SJ Amsterdam, The Netherlands. E-mail: joostw@wins.uva.nl.
- L.J. van Vliet, P.W. Verbeek, and M. van Ginkel are with the Pattern Recognition Group of the Faculty of Applied Sciences, Delft University of Technology, Lorentzweg 1, 2628 CJ Delft, The Netherlands. E-mail: {L.J.vanVliet, P.W.Verbeek, michael}@ph.tn.tudelft.nl.

Manuscript received 22 July 1999; revised 2 Aug. 2000; accepted 17 Jan. 2001. Recommended for acceptance by S. Sarkar. For information on obtaining reprints of this article, please send e-mail to: tpami@computer.org, and reference IEEECS Log Number 110288.

The requirement for two orthonormal transformation functions poses an unnecessary limitation to the symmetries. For example, such a set of functions does not exist for the parabolic model we propose, i.e., parabolic isophotes along a linearly increasing symmetry axis. We extend his method by noting that only the existence of the differential fields of the two transformation functions is essential.

2 ORIENTED PATTERNS

An oriented pattern $m(x, y)$ can be written as a real one dimensional function g of a model function u

$$m(x, y) = g(u(x, y, \mathbf{a})). \quad (1)$$

The model function $u(x, y, \mathbf{a})$ describes the shape of the isophotes and a contains local isophote parameters such as orientation and curvature. Consequently, the gradient (differential field) of m ,

$$\nabla m = \frac{dg}{du} \nabla u, \quad (2)$$

is a dg/du weighted version of the gradient of u . In oriented patterns, we distinguish between two perpendicular orientations; along the isophote (tangent) and along the gradient. Note that orientation is defined on the interval $[0, \pi)$. Consequently, vectors in opposite directions have the same orientation.

Consider the function $f(x, y)$ representing a local image (window) and a model function $u(x, y, \mathbf{a})$. It is of interest to what extent $f(x, y)$ is described by the model function $u(x, y, \mathbf{a})$. This is measured by decomposing the derivative energy of $f(x, y)$ into two contributions, one parallel and one perpendicular to the normalized differential field of $u(x, y, \mathbf{a})$. This results in the following energies:

$$\begin{aligned} E_f(\mathbf{a}) &= \int \int \left(\nabla f \cdot \frac{\nabla u(\mathbf{a})}{\|\nabla u(\mathbf{a})\|} \right)^2 dx dy, \\ E_r(\mathbf{a}) &= \int \int \left(\nabla f \cdot \frac{(\nabla u(\mathbf{a}))_{\perp}}{\|\nabla u(\mathbf{a})\|} \right)^2 dx dy, \end{aligned} \quad (3)$$

where $E_f(\mathbf{a})$ denotes the fit energy and $E_r(\mathbf{a})$ the residual energy. The subscript \perp indicates a rotation of 90° of the vector and the integrals represent the averaging over the local image. A quality measure of the fit can be found by comparing the fit energy with the residual energy. Since no a priori knowledge exists to interpret the energy difference between the fit and the residual energy, we normalize the difference with the total gradient energy to obtain the following quality measure $c(\mathbf{a})$:

$$c(\mathbf{a}) = \frac{E_f(\mathbf{a}) - E_r(\mathbf{a})}{E_f(\mathbf{a}) + E_r(\mathbf{a})} \quad -1 \leq c \leq 1. \quad (4)$$

The value of $c(\mathbf{a})$ varies from -1 for a pattern of which the isophotes are exactly perpendicular to those of the model function $u(x, y, \mathbf{a})$ and +1 for a pattern which is exactly described by the model function. The isotropic noise energy is distributed equally between the fit and the residual energy.

More important than the quality measure for an arbitrary \mathbf{a} is to know which \mathbf{a} maximizes the quality function c , i.e., maximizes E_f and minimizes E_r . The vector \mathbf{a} contains model parameters which describe local features. Therefore, optimizing the confidence function c corresponds to feature estimation. Furthermore, the

quality measure $c(\mathbf{a})$ informs us about the success of the fit and can be seen as a confidence measure of the estimated features. Besides comparing confidence measures of the same model function, it is also possible to compare confidence measures of different model functions. Note that the normalization of the confidence measures is independent of the model function. By comparing optimized confidence functions of various models, one can find out which model describes the local pattern best.

Usually, the complexity of the confidence function does not allow a closed-form solution of the optimization criterion. The straight model is an exception. In the case of curvilinear models, we avoid costly (iterative) optimization procedures by considering approximate confidence functions which do allow closed-form solutions.

3 STRAIGHT-ORIENTED PATTERNS

Locally, many oriented patterns can be characterised by a straight model. For such a pattern the model function $u(x, y, \mathbf{a})$ is given by

$$u(x, y, \phi) = x \cos \phi + y \sin \phi, \quad (5)$$

with ϕ the orientation perpendicular to the model isophotes. Substituting this in (3) yields

$$E_f(\phi) = \frac{1}{2} (\overline{f_x^2} + \overline{f_y^2}) + \frac{1}{2} (\overline{f_x^2} - \overline{f_y^2}) \cos 2\phi + \frac{1}{2} \overline{2f_x f_y} \sin 2\phi. \quad (6)$$

A bar ($\overline{\bullet}$) denotes an averaged quantity and will from now on replace the integrals responsible for averaging over a local image. The confidence value $c(\phi)$ is

$$c(\phi) = \frac{1}{\overline{f_x^2} + \overline{f_y^2}} \left((\overline{f_x^2} - \overline{f_y^2}) \cos 2\phi + \overline{2f_x f_y} \sin 2\phi \right). \quad (7)$$

$c(\phi)$ can be maximized as a function of the orientation ϕ . This yields the following (gradient-based) orientation estimator [1], [2], [3], [4]:

$$\phi_{opt} = \frac{1}{2} \arctan \frac{\overline{2f_x f_y}}{\overline{f_x^2} - \overline{f_y^2}}. \quad (8)$$

with confidence value $c(\phi_{opt})$:

$$c(\phi_{opt}) = \frac{d^2}{g^2}, \quad \text{where } d^4 = \overline{f_x^2} - \overline{f_y^2}^2 + \overline{2f_x f_y}^2. \quad (9)$$

This confidence measure can also be interpreted as a measure for translation invariance and shows an intuitive dependency to the pattern orientation ϕ_{opt} .

$$\begin{aligned} c(\phi) &= \frac{d^2 (\cos^2(\phi - \phi_{opt}) - \sin^2(\phi - \phi_{opt}))}{g^2} \\ &= \frac{1}{2} c(\phi_{opt}) (1 + \cos(2(\phi - \phi_{opt}))). \end{aligned} \quad (10)$$

The maximum of the confidence measure $c(\phi_{opt})$ reduces due to noise in the local image f . For a linear pattern p distorted by additive uncorrelated noise n ($f = p + n$), the confidence value $c(\phi_{opt})$ is:

$$c(\phi_{opt}) = \frac{d^2}{\|\nabla f\|^2} = \frac{d^2}{\|\nabla p + \nabla n\|^2} = \frac{d^2}{\|\nabla p\|^2} \frac{\|\nabla p\|^2}{\|\nabla p\|^2 + \|\nabla n\|^2}. \quad (11)$$

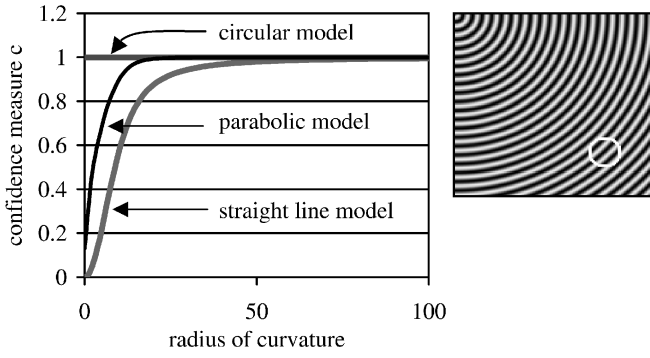


Fig. 1. Confidence measure $c(\hat{\phi}, \hat{\kappa})$ of circular, parabolic, and straight line models on a noise-free pattern of concentric circles.

Note that the gradient noise energy is divided equally over E_f and E_r . Therefore, the numerator of c is unaffected by noise. Noise increases the total gradient energy (denominator of c), which lowers the confidence value $c(\hat{\phi}_{opt})$. Another reason for a lower confidence value is a deviation between the local image and the model function. For instance when curved lines occur, then curvature will contribute to E_r . In the next section, we will extend the model to include curved patterns.

4 CURVED ORIENTED PATTERNS

We present two model functions which locally model curved oriented patterns. A parabolic model

$$u(x, y, \phi, \kappa) = \frac{1}{2} \kappa w^2 - v \quad (12)$$

and a concentric circle model

$$u(x, y, \phi, \kappa) = \sqrt{\kappa^2 w^2 + (1 - \kappa v)^2} \quad (13)$$

in which κ is the curvature. The Gauge coordinates v, w are obtained by

$$v = x \cos \phi + y \sin \phi \quad w = -x \sin \phi + y \cos \phi \quad (14)$$

Here, we discuss the parabolic approximation. For the circular approximation, we refer to Appendix A. Using the parabolic model function and (3), the following energies are obtained:

$$\begin{aligned} E_f(\phi, \kappa) &= \frac{\kappa^2 w^2 f_w^2 - 2\kappa w f_v f_w + f_v^2}{1 + \kappa^2 w^2}, \\ E_r(\phi, \kappa) &= \frac{\kappa^2 w^2 f_v^2 + 2\kappa w f_v f_w + f_w^2}{1 + \kappa^2 w^2}, \end{aligned} \quad (15)$$

where f_v and f_w are the derivatives in, respectively, the v and w direction. Finding the curvature and orientation that maximize the confidence function requires a search in ϕ, κ -space. In this paper, we shall not further investigate this method due to its high computational demands. Instead, we propose a way to approximate the confidence function, allowing a fast closed-form solution.

An approximation to the orientation ϕ can be obtained by looking at the axis of minimal translation invariance for parabolic and circular patterns. In the case of a circular pattern, this is the v -axis. For a parabolic pattern, it depends on the curvature and the window size used. For small curvatures (i.e., compared to the window size), the minimal translation invariant axis is equal to the w -axis. Increasing the curvature, the axis of minimal translation

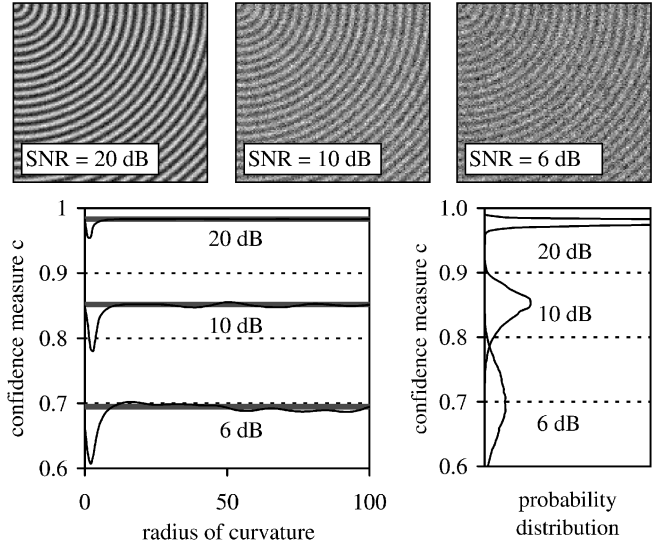


Fig. 2. (a) Average confidence measure $c(\hat{\phi}, \hat{\kappa})$ for the circular model as a function of the radius for three different SNRs (top to bottom: 20 dB, 10 dB, 6 dB). The measure $c(\hat{\phi}, \hat{\kappa})$ yields a small bias for small radii. The horizontal lines indicate the average confidence measure for, straight model for the corresponding SNR. (b) Probability density functions of the confidence measure for the straight-oriented patterns for the three different SNRs (top to bottom: 20 dB, 10 dB, 6 dB).

invariance jumps to the w -axis. Therefore, an approximation of the orientation needed to determine the v and w -axes in (15) can be computed with (8). After substituting the orientation, the resulting equations only depend on the curvature. Iterative maximization of the confidence function in κ -space is still time-consuming. We propose approximating this maximum by using locally adapted weighting. The weighting function of E_f and E_r (denoted by the bar $\bar{\bullet}$) is in its turn weighted by $(1 + \kappa^2 w^2)$ after which we normalize for this weighting. This mathematical trick has a high resemblance to normalized convolution [14]. It results in

$$\begin{aligned} \hat{E}_f(\kappa) &= \frac{\kappa^2 \bar{w}^2 \bar{f}_w^2 - 2\kappa \bar{w} \bar{f}_v \bar{f}_w + \bar{f}_v^2}{1 + \kappa^2 \bar{w}^2}, \\ \hat{E}_r(\kappa) &= \frac{\kappa^2 \bar{w}^2 \bar{f}_v^2 + 2\kappa \bar{w} \bar{f}_v \bar{f}_w + \bar{f}_w^2}{1 + \kappa^2 \bar{w}^2}. \end{aligned} \quad (16)$$

A hat ($\hat{\bullet}$) above a quantity indicates an approximation. Since the fit energy E_f might be a function of the coordinate w , as is the adapted weighting function, optimization lead to a false curvature estimate. Therefore, minimization of the residual energy E_r is used to find the following closed-form curvature estimate:

$$\hat{\kappa} = \frac{\bar{w}^2 \bar{f}_v^2 - \bar{w}^2 \cdot \bar{f}_w^2 - \sqrt{4\bar{w}^2 \cdot \bar{w} \bar{f}_v \bar{f}_w^2 + (-\bar{w}^2 \bar{f}_v^2 + \bar{w}^2 \cdot \bar{f}_w^2)^2}}{2\bar{w}^2 \cdot \bar{w} \bar{f}_v \bar{f}_w}. \quad (17)$$

The confidence measure can now be computed in two different ways. The confidence measure $c(\phi, \kappa)$ has its maximum at $\hat{\phi}_{opt}, \hat{\kappa}_{opt}$. To avoid an iterative search for this optimum, one can compute $c(\hat{\phi}, \hat{\kappa})$ by substituting $\hat{\phi}$ and $\hat{\kappa}$ in (15) and (4). Note that estimates $\hat{\phi}$ and $\hat{\kappa}$ do not have to be equal to the values of ϕ and κ that optimize the confidence function. However, computing $c(\hat{\phi}, \hat{\kappa})$ is still expensive. A significant speed-up can be obtained by approximating the confidence measure using the approximate energies of (16).

$$\hat{c}(\phi, \kappa) = \frac{\hat{E}_f(\phi, \kappa) - \hat{E}_r(\phi, \kappa)}{\hat{E}_f(\phi, \kappa) + \hat{E}_r(\phi, \kappa)}. \quad (18)$$

Again, one can avoid an iterative search by substituting $\hat{\phi}$ and $\hat{\kappa}$ in (18), which yield $\hat{c}(\hat{\phi}, \hat{\kappa})$.

The curvature estimator in (17) is the tangential or isophote curvature. The normal (or gradient flow line) curvature [17] can be computed by exchanging the v and w coordinates in (12) and (13).

5 IMPLEMENTATION

Direct computation of the curvature and the confidence measure is a space-variant operation. This yields a high computational demand. Fortunately, (16) to (18) can be calculated with global convolutions which can be implemented by multiplication in the Fourier-domain. This yields a substantial reduction in computational complexity. The derivatives f_x and f_y are implemented as regularized derivative filters:

$$f_x \equiv f(x, y) \otimes \frac{\partial g(x, y; \sigma_g)}{\partial x} \xrightarrow{F} j\omega_x \tilde{f}(\omega_x, \omega_y) \tilde{g}(\omega_x, \omega_y; \sigma_g), \quad (19)$$

with \tilde{f} the Fourier transform of f and $g(x, y; \sigma_g)$ a Gaussian regularization function of scale σ_g .

$$g(x, y; \sigma_g) = \frac{1}{2\pi\sigma_g^2} e^{-(x^2+y^2)/2\sigma_g^2} \xrightarrow{F} \tilde{g}(\omega_x, \omega_y; \sigma_g) = e^{-\frac{1}{2}(\omega_x^2+\omega_y^2)\sigma_g^2}. \quad (20)$$

The terms of the curvature estimator and the confidence measure, (16) and (17), are expanded in Appendix B (the circular model is treated in Appendix A). The remaining terms $\overline{x^p y^q f_x^r f_y^s}$ are conveniently calculated as multiplications in the Fourier domain

$$\overline{x^p y^q f_x^r f_y^s} = u(p, q, \sigma_a) \otimes f_x^r f_y^s \xrightarrow{F} \tilde{u}(p, q, \sigma_a) F \left\{ f_x^r f_y^s \right\}. \quad (21)$$

For the window function, we choose a Gaussian of scale σ_a . The Fourier transform of the filter $u()$ is

$$u(p, q, \sigma_a) \equiv x^p y^q g(x, y; \sigma_a) \xrightarrow{F} \tilde{u}(p, q, \sigma_a) \equiv j^{p+q} \frac{\partial^{p+q} \tilde{g}(\omega_x, \omega_y; \sigma_a)}{\partial \omega_x^p \partial \omega_y^q}. \quad (22)$$

Due to the high frequency character of oriented patterns, σ_g should be kept small, i.e., tuned to the frequency characteristics of the cross-section of a line. Noise suppression is accomplished by averaging all terms by Gaussian window (size σ_a), i.e., the size of the curvilinear model.

6 EXPERIMENTS

In this section the proposed algorithms are tested on synthetic and real-world images. The feature extraction which we presented is based upon finding a maximum of the confidence measure in parameter space $c(a)$. The curvature of oriented patterns corresponds to the position of the maximum in $c(\kappa, \phi)$ -space. To avoid searching κ, ϕ -space, the approximations $\hat{\phi}$ and $\hat{\kappa}$ are proposed. With these, an approximated confidence measure \hat{c} and the exact confidence measure c may be computed. The goal of the experiments is to investigate the performance of these approximations as a function of the curvature. Also, the robustness with respect to the noise is checked. The tests are performed on a concentric circle image $f(x, y) = \sin(\sqrt{x^2 + y^2} + \varphi) + n$ (see Fig. 1) in which $n = N(0, \sigma_n^2)$ and φ is a phase-term set randomly for

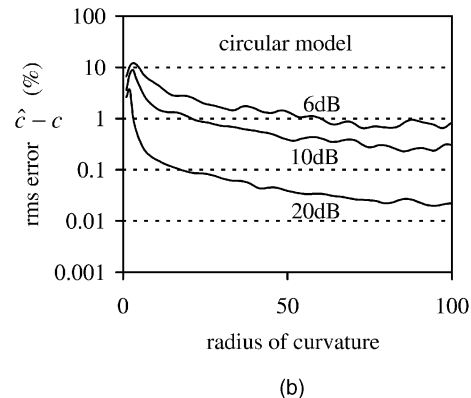
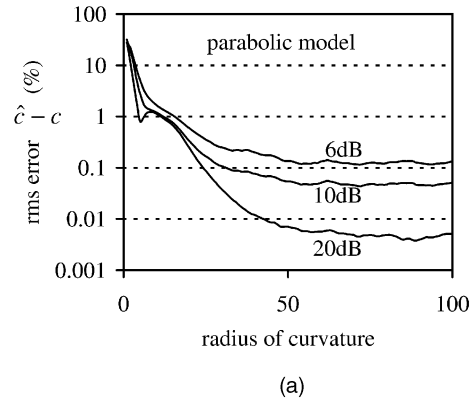


Fig. 3. Rms error between the actual confidence measure and its approximation as a function of the radius. (a) Approximate parabolic model applied to concentric circle patterns of various SNR (top-to-bottom: 6 dB, 10 dB, 20 dB). (b) Approximate circular model applied to concentric circle patterns of various SNR (top-to-bottom: 6 dB, 10 dB, 20 dB).

every noise-realization. For the signal-to-noise ratio, we use $SNR = 10 \log(h^2/\sigma_n^2)$, where h is the contrast difference and σ_n the standard deviation of the noise. Be aware that the proposed algorithms are based on the gradient energy of the local image. Thus, an increase of the pattern frequency will usually result in a higher SNR (gradient energy versus filtered noise variance) and, therefore, a better performance. All experiments on the concentric circle image are based on 100 measurements. Unless mentioned otherwise the sigma sizes are $\sigma_g = 1.0$ and $\sigma_a = 5.0$.

Confidence measure as selection criterion. The importance of choosing the right model is illustrated in Fig. 1, which shows the confidence measures of the circular, parabolic, and straight model applied to a noise-free pattern of concentric circles. It is clear that, for high curvatures, the deviation of the straight and the parabolic model from the circle pattern results in a significantly lower value of the confidence measure.

Bias of the actual confidence measure. To investigate to what extent the optimum of the confidence function in κ, ϕ -space is found, we compare the average confidence measure of the circular model applied to curved patterns with the average confidence measure of a straight model applied to a straight pattern. Both images have identical signal-to-noise ratios. The confidence measure $c(\phi, \kappa)$ of a curvilinear model can be slightly higher than the confidence measure of a straight model. This slight increase is

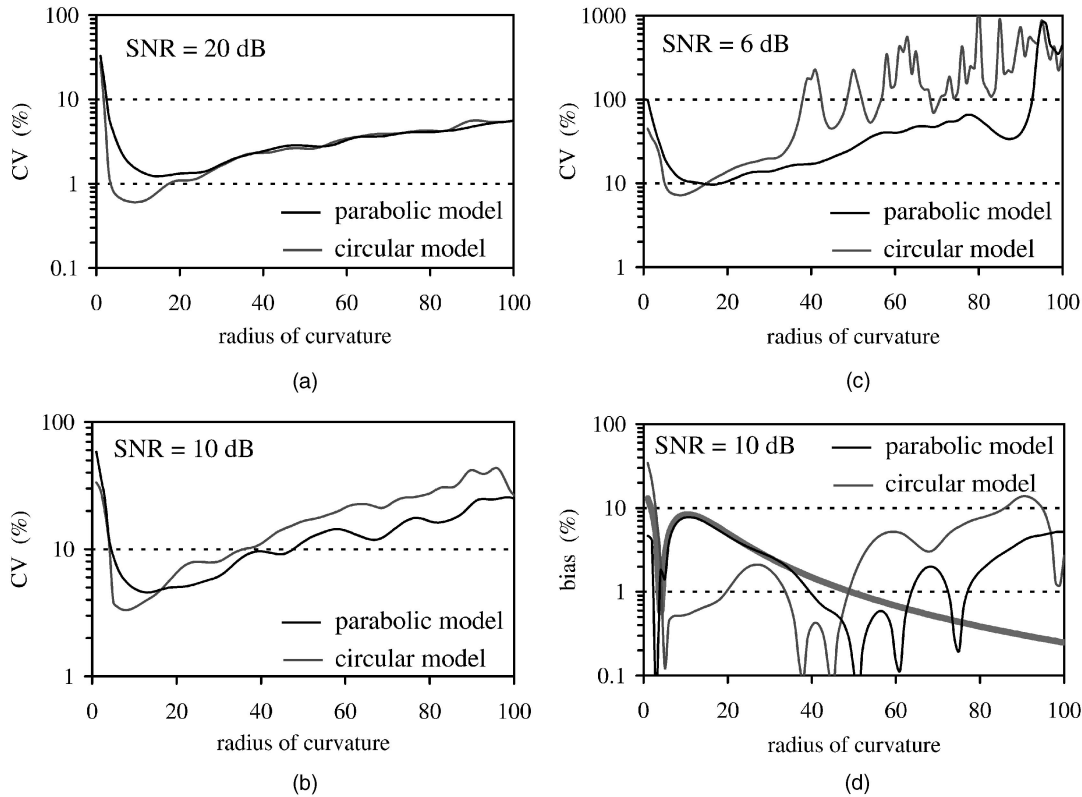


Fig. 4. Curvature estimators using curvilinear models: black line = parabolic model, gray line = circular model. (a), (b) and (c) Coefficient-of-variation (CV) for the parabolic and circular model-based curvature estimators for different SNR (20 dB, 10 dB, 6 dB). (d) Bias of parabolic and circular model based curvature estimators (SNR = 10 dB) (thick gray line indicates the noise-free bias of curvature using the parabolic model).

caused by the fact that the curved model allows for two parameters to adjust to the noise.

The average confidence measure $c(\hat{\phi}, \hat{\kappa})$ of the circular model applied to the concentric circles is depicted in Fig. 2 for three SNR's (20dB, 10dB, 6dB). It clearly shows that, for small radii, the average confidence measure $c(\hat{\phi}, \hat{\kappa})$, decreases. This is caused by an increasing discrepancy between the approximated $(\hat{\phi}, \hat{\kappa})$ and the optimal $(\phi_{opt}, \kappa_{opt})$ for small radii. Note, $c(\phi_{opt}, \kappa_{opt})$ does not decrease for small radii. Fig. 2b indicates the variation around the average confidence measure for the straight model. Increasing the window size (local image) reduces the variation in exchange of a further decrease of $c(\hat{\phi}, \hat{\kappa})$ for small radii.

Approximation error of the confidence measure. In Section 4, we presented two methods for computing the confidence measure, the actual confidence measure $c(\hat{\phi}, \hat{\kappa})$ and an approximation $\hat{c}(\hat{\phi}, \hat{\kappa})$. In Fig. 3, the rms (root-mean-square) error due to this approximation is depicted for the circular and the parabolic model. For both models, these errors are small. Only for high curvatures (small radii), it may be worthwhile to compute the actual confidence measure.

Robustness of the curvature estimator. It is important to test the robustness of the curvature estimation. In Fig. 4, the noise sensitivity of the parabolic and circular curvature estimators is depicted. Both models were applied to the concentric circles. The coefficient-of-variation ($CV = \sigma/\mu$) of both models is similar for the middle and high SNRs, but the parabolic models performs better for low SNRs. Considering the advantage of the circular curvature estimator due to the exact match between the model and the pattern, we show that the parabolic curvature estimator suffers

less from the approximations. The parabolic curvature estimator performs at least as well over a wide range of curvatures. Only for high curvatures, the circular model can take advantage of the exact match. In practice, one can compute the curvature corresponding to both models. The one with the highest confidence measure is preferred because its model yields a better description of the data.

Application of curvilinear models to real-world data sets. In Fig. 5, an interference pattern, together with the curvature and confidence estimation for both the parabolic and circular model, is depicted. As expected, the parabolic model fails in the middle of the ellipses, as indicated by an abrupt drop of the confidence measure. The circular confidence measure hardly decreases for the circles at the top and the bottom of the image. For the flatter ellipses on the left and the right, the mismatch between the model and the pattern is slightly larger. In the difference image between the circular and parabolic confidence measures, the lighter areas indicate a better description of the circular model, whereas, in the darker areas, the parabolic model yields a better fit. The slightly darker lines denote an almost perfect parabolic line pattern. The isophote curvature fails at the ridges (dark lines) and valleys (white lines) as expected (see Section 1).

The estimated local curvature of a fingerprint and a CT cross-section of a tree-trunk are depicted in Fig. 6. Both curvilinear models produced similar results. The dark lines in the logarithmically stretched curvature images denote locally straight patterns. Both peaks in the fingerprints curvature correspond to important minutia for fingerprint recognition [15], [16]. The isophote

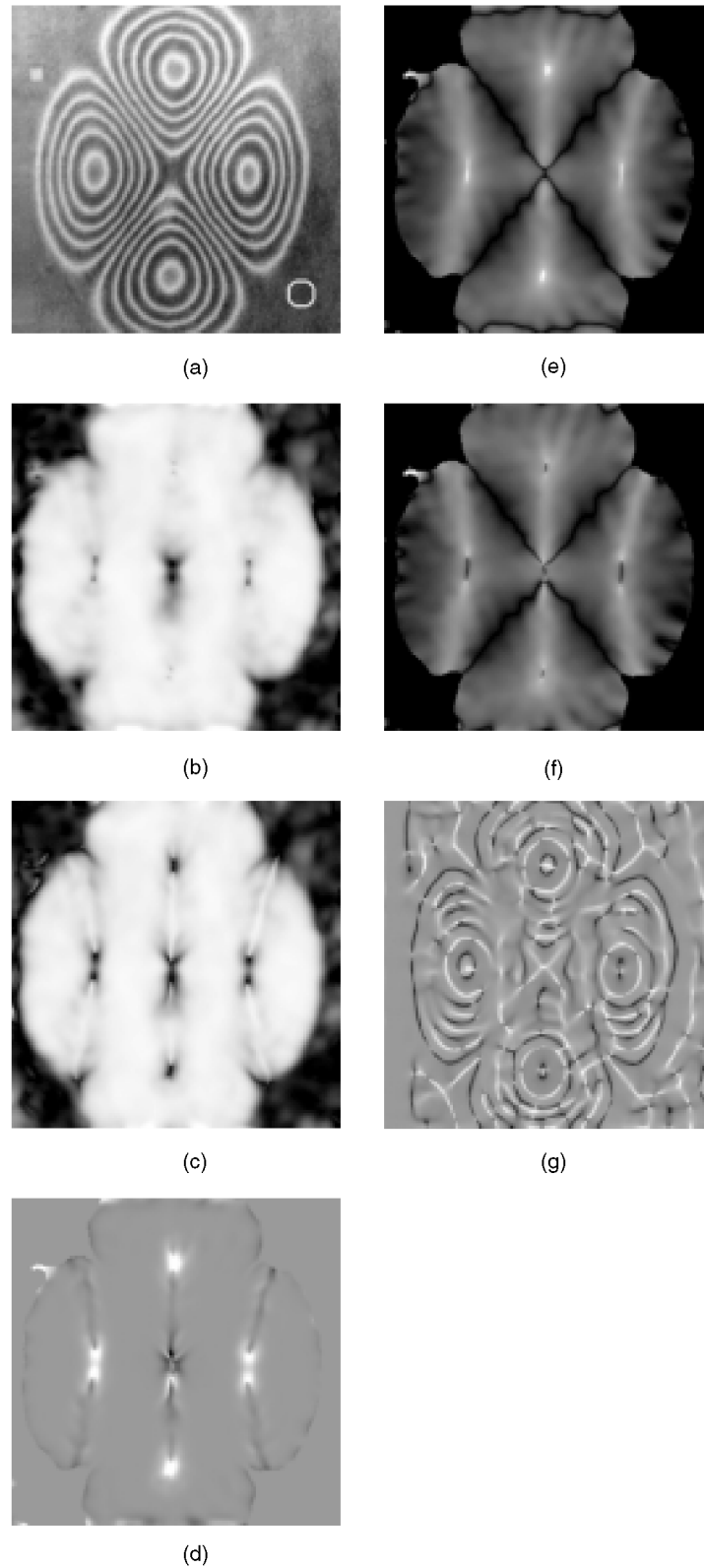


Fig. 5. (a) Interference pattern of a vibrating plate. The superimposed circle denotes the size of the curvilinear model. (b) and (c) Confidence measures for, respectively, the circular and parabolic model (range $[0,1]$) computed with $\sigma_g = 1.0$ and $\sigma_a = 5.0$. (d) Difference in confidence measure between circular and parabolic model (range $[-0.5, 0.5]$). (e) and (f) Estimated curvatures $\hat{\kappa}$ for respectively the circular and parabolic model (log stretched). (g) Isophote curvature at scale $\sigma = 5$ (range $[-1,1]$).

curvature fails at the ridges (dark lines) and valleys (white lines) as expected (see Section 1). The curvilinear curvature can be used to improve (to prevent jumping the rails) the ridge tracking [16],

which is already based on orientation estimation. The high confidence measures (white areas in confidence images) indicate a perfect fit of the model and a reliable curvature estimate.

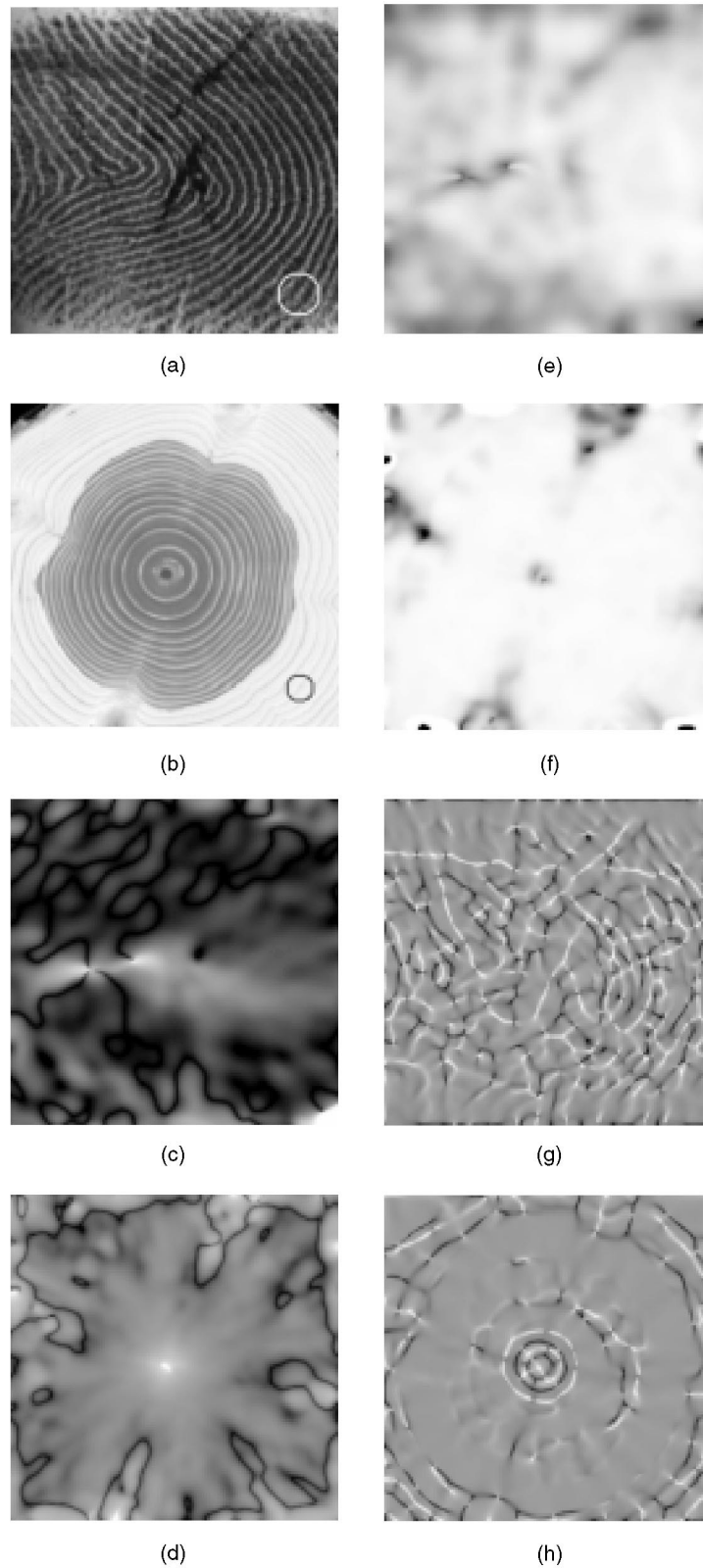


Fig. 6. (a) Fingerprint image. (b) CT image of trunk. (c) and (d) The estimated curvature $\hat{\kappa}$ using the parabolic model (log stretched) at $\sigma_g = 1.0$ and $\sigma_a = 5.0$. (e) and (f) The confidence measure of the parabolic model (range [0, 1]), (g) and (h) Isophote curvature at scale $\sigma = 5$ (range [-1, 1]).

7 CONCLUSIONS

In this paper, we present a method to compare a local image with a model function. A quality measure indicates the resemblance between the local image and the model function. Feature extraction

is obtained by optimization of the quality function as a function of the parameters which represent the feature. The quality function is interpreted as a confidence measure for the measured features. We propose two curvilinear models to describe curved oriented

patterns. To avoid searching ϕ, κ -space, we propose, closed-form solution for approximations to the actual parameters of the curvilinear models $\hat{\phi}$ and $\hat{\kappa}$. Instead of the exact confidence measure $c(\hat{\phi}, \hat{\kappa})$ an approximation $\hat{c}(\hat{\phi}, \hat{\kappa})$, can be computed resulting in a huge reduction in computational demand. We demonstrate that these approximations yield good results for almost all curvatures. Only for the highest curvatures, one might decide to compute $c(\hat{\phi}, \hat{\kappa})$ or (even more computationally demanding) to iterate in ϕ, κ -space for $c(\phi_{opt}, \kappa_{opt})$.

APPENDIX A

For a concentric circle model, $u(x, y, \phi, \kappa) = \sqrt{\kappa^2 w^2 + (1 - \kappa v)^2}$, the fit and residual energies are

$$E_f(\kappa) = \frac{\overline{(1 - \kappa v)^2 f_v^2 - 2\kappa w(1 - \kappa v)f_v f_w + \kappa^2 w^2 f_w^2}}{(1 - \kappa v)^2 + \kappa^2 w^2} \quad (23)$$

$$E_r(\kappa) = \frac{\overline{(1 - \kappa v)^2 f_w^2 + 2\kappa w(1 - \kappa v)f_v f_w + \kappa^2 w^2 f_v^2}}{(1 - \kappa v)^2 + \kappa^2 w^2}.$$

To obtain a closed-form solution for the curvature and the confidence measure, the local energies are computed inside a $(\kappa^2 w^2 + (1 - \kappa v)^2)$ -weighted space-variant window. This yields

$$\hat{E}_f = \frac{\kappa^2 \overline{(v^2 f_v^2 + 2v w f_v f_w + w^2 f_w^2)} + 2\kappa \overline{(-v f_v^2 - w f_v f_w)} + \overline{f_v^2}}{1 - 2\kappa \bar{v} + \kappa^2 \overline{(v^2 + w^2)}} \quad (24)$$

$$\hat{E}_r = \frac{\kappa^2 \overline{(v^2 f_w^2 - 2v w f_v f_w + w^2 f_v^2)} + 2\kappa \overline{(-v f_w^2 + w f_v f_w)} + \overline{f_w^2}}{1 - 2\kappa \bar{v} + \kappa^2 \overline{(v^2 + w^2)}}$$

$$\equiv \frac{E\kappa^2 + 2F\kappa + G}{1 + D\kappa^2},$$

with $\bar{v} = 0$. The minimization of the residual energy yields an approximation of the curvature:

$$\hat{\kappa} = \frac{E - GD - \sqrt{4F^2 D + (-E + GD)^2}}{2FD}. \quad (25)$$

The terms of \hat{E}_f and \hat{E}_g are expanded with (14) and

$$f_v = f_x \cos \phi + f_y \sin \phi \quad f_w = -f_x \sin \phi + f_y \cos \phi. \quad (26)$$

This results in

$$\begin{cases} A = \overline{x^2 f_x^2 + 2xy f_x f_y + y^2 f_y^2} \\ B = -\overline{(x f_x^2 + y f_x f_y) \cos \phi - (x f_x f_y + y f_y^2) \sin \phi} \\ C = \overline{f_x^2 \cos^2 \phi + 2f_x f_y \cos \phi \sin \phi + f_y^2 \sin^2 \phi} \\ D = 2\sigma_a^2 \\ E = \overline{x^2 f_y^2 - 2xy f_x f_y + y^2 f_x^2} \\ F = \overline{(y f_x f_y - x f_y^2) \cos \phi + (x f_x f_y - y f_x^2) \sin \phi} \\ G = \overline{f_y^2 \cos^2 \phi - 2f_x f_y \cos \phi \sin \phi + f_x^2 \sin^2 \phi}. \end{cases} \quad (27)$$

The averaged terms can be computed as global convolutions (see Section 5). The approximated confidence function is computed with

$$\hat{c} = \frac{\kappa^2(A - E) + 2\kappa(B - F) + (C - G)}{\kappa^2(A + E) + 2\kappa(B + F) + (C + G)}. \quad (28)$$

APPENDIX B

The terms for the parabolic confidence measure (16) and curvature estimator (17) are

$$\begin{cases} w^2 \overline{f_w^2} = \overline{y^2 f_y^2} \cos^4 \phi - 2 \overline{(xy f_y^2 + y^2 f_x f_y)} \cos^3 \phi \sin \phi \\ + \overline{(x^2 f_y^2 + 4xy f_x f_y + y^2 f_x^2)} \cos^2 \phi \sin^2 \phi \\ + 2 \overline{(-x^2 f_x f_y - xy f_y^2)} \cos \phi \sin^3 \phi + \overline{x^2 f_x^2} \sin^4 \phi \\ \overline{w^2 f_v^2} = \overline{y^2 f_x^2} \cos^4 \phi - 2 \overline{(xy f_x^2 - y^2 f_x f_y)} \cos^3 \phi \sin \phi \\ + \overline{(x^2 f_x^2 - 4xy f_x f_y + y^2 f_y^2)} \cos^2 \phi \sin^2 \phi \\ + 2 \overline{(x^2 f_x f_y - xy f_y^2)} \cos \phi \sin^3 \phi + \overline{x^2 f_y^2} \sin^4 \phi \\ \overline{w f_v f_w} = \overline{y f_x f_y} \cos^3 \phi + \overline{(-x f_x f_y - y(f_x^2 - f_y^2))} \cos^2 \phi \sin \phi \\ + \overline{(x(f_x^2 - f_y^2) - y f_x f_y)} \cos \phi \sin^2 \phi + \overline{x f_x f_y} \sin^3 \phi \\ \overline{w^2} = \sigma_a^2 \end{cases} \quad (29)$$

for $\overline{f_v^2}$ and $\overline{f_w^2}$, see term, C and G in Appendix A.

ACKNOWLEDGMENTS

The research was performed while J. van de Weijer was with the Delft University of Technology. This work was partially supported by the Royal Netherlands Academy of Arts and Sciences (KNAW) and the Rolling Grants program of the Foundation for Fundamental Research in Matter (FOM).

REFERENCES

- [1] M. Kass and A. Witkin, "Analyzing Oriented Patterns," *Computer Vision, Graphics, and Image Processing*, vol. 37, pp. 362-385, 1987.
- [2] J. Bigun, G.H. Granlund, and J. Wiklund, "Multidimensional Orientation Estimation with Applications to Texture Analysis and Optical Flow," *IEEE Trans. Pattern Analysis and Machine Intelligence*, vol. 13, pp. 775-790, 1991.
- [3] L. Haglund, "Adaptive Multi-Dimensional Filtering," Linköping Univ., Sweden, 1992.
- [4] L.J. van Vliet and P.W. Verbeek, "Estimators for Orientation and Anisotropy in Digitized Images," *Proc. First Conf. Advanced School for Computing and Imaging*, pp. 442-450, 1995.
- [5] P.W. Verbeek, L.J. van Vliet, and J. van de Weijer, "Improved Curvature and Anisotropy Estimation for Curved Line Bundles," *Proc. 14th Int'l Conf. Pattern Recognition*, pp. 528-533, 1998.
- [6] M. Worring and A.W.M. Smeulders, "Digital Curvature Estimation," *CVGIP: Image Understanding*, vol. 58, pp. 366-382, 1993.
- [7] P.W. Verbeek, "A Class of Sampling-Error Free Measures in Oversampled Band-Limited Images," *Pattern Recognition Letters*, vol. 3, pp. 287-292, 1985.
- [8] L.J. van Vliet and P.W. Verbeek, "Curvature and Bending Energy in 2D and 3D Digitized Images," *Proc. Eighth Scandinavian Conf. Image Processing, SCIA '93*, pp. 1403-1410, 1993.
- [9] M. van Ginkel, P.W. Verbeek, and L.J. van Vliet, "Curvature Estimation for Overlapping Curved Patterns Using Orientation Space," *Proc. Fourth Conf. Advanced School for Computing and Imaging*, pp. 173-178, 1998.
- [10] M. van Ginkel, J. van de Weijer, L.J. van Vliet, and P.W. Verbeek, "Curvature Estimation from Orientation Fields," *Proc. 11th Scandinavian Conf. Image Analysis, SCIA '99*, 1999.
- [11] J. Hansen and J. Bigun, "Local Symmetry Modeling Multi-Dimensional Images," *Pattern Recognition Letters*, vol. 13, pp. 253-262, 1992.
- [12] J. Bigun and M.H. du Buf, "Symmetry Interpretation of Complex Moments and the Local Power Spectrum," *J. Visual Comm. and Image Representation*, vol. 6, pp. 154-163, 1995.
- [13] J. Bigun, "Pattern Recognition in Images by Symmetry and Coordinate Transformations," *Computer Vision and Image Understanding*, vol. 68, pp. 290-307, 1997.
- [14] H. Knutsson and C.-F. Westin, "Normalised Convolution: A Technique for Filtering Incomplete and Uncertain Data," *Proc. Eighth Scandinavian Conf. Image Processing, SCIA '93*, 1993.
- [15] D. Maio and D. Maltoni, "Direct Gray-Scale Minutiae Detection in Fingerprints," *IEEE Trans. Pattern Analysis and Machine Intelligence*, vol. 19, pp. 27-40, 1997.
- [16] A. Jain, L. Hong, and R. Bolle, "On-Line Fingerprint Verification," *IEEE Trans. Pattern Analysis and Machine Intelligence*, vol. 19, pp. 302-314, 1997.
- [17] P. Breton and S.W. Zucker, "Shadows and Shading Flow Fields," *Proc. IEEE Conf. Computer Vision and Pattern Recognition CVPR '96*, pp. 782-789, 1996.

